Check for updates

View Article Online
View Journal

Soft Matter

Accepted Manuscript

This article can be cited before page numbers have been issued, to do this please use: L. Gomez, N. A. García and T. Pöschel, *Soft Matter*, 2023, DOI: 10.1039/D3SM00148B.

This is an Accepted Manuscript, which has been through the Royal Society of Chemistry peer review process and has been accepted for publication.

Accepted Manuscripts are published online shortly after acceptance, before technical editing, formatting and proof reading. Using this free service, authors can make their results available to the community, in citable form, before we publish the edited article. We will replace this Accepted Manuscript with the edited and formatted Advance Article as soon as it is available.

You can find more information about Accepted Manuscripts in the Information for Authors.

Please note that technical editing may introduce minor changes to the text and/or graphics, which may alter content. The journal's standard Terms & Conditions and the Ethical guidelines still apply. In no event shall the Royal Society of Chemistry be held responsible for any errors or omissions in this Accepted Manuscript or any consequences arising from the use of any information it contains.

ROYAL SOCIETY OF CHEMISTRY

rsc.li/soft-matter-journal

View Article Online
DOI: 10.1039/D3SM00148B

Soft Matter

ARTICLE TYPE

Cite this: DOI: 00.0000/xxxxxxxxxx

Macroscopic Analogue to Entangled Polymers

Leopoldo R. Gómez,*[a,b] Nicolás A. García,[b,c] and Thorsten Pöschel[a]

Received Date
Accepted Date

DOI: 00.0000/xxxxxxxxxx

The entangled structure of polymeric materials is often described as resembling a bowl of spaghetti, swarms of earthworms, or snakes. These analogies not only illustrate the concept, but form the foundation of polymer physics. However, the similarity between these macroscopic, athermal systems and polymers in terms of topology remains uncertain. To better understand this relationship, we conducted an experiment using X-ray tomography to study the structure of arrays of linear rubber bands. We found that, similar to linear polymers, the average number of entanglements increases linearly with the length of the ribbons. Additionally, we observed that entanglements are less frequent near the surface of the container, where there are also more ends, similar to what has been seen in trapped polymers. These findings provide the first experimental evidence supporting the visualization of polymer structures using macroscopic, athermal analogues, confirming the initial intuitive insights of the pioneers of polymer physics.

Published on 24 April 2023. Downloaded on 4/26/2023 11:22:33 PM.

Soft Matter Accepted Manuscript

Introduction: The entangled structure of polymer melts, made of disordered and tangled assemblies of long molecules, has often been compared to a plate of noodles or a swarm of earthworms or snakes (Figure 1a)[1,2]. With this mental image, Edwards and de Gennes developed a description of the configurations and motions of polymer chains in melts, introducing the concept of confining tubes and reptation dynamics (Figure 1b-c)[1–3]. The reference chain is confined to a tubular region defined by neighboring chains, and as a result, linear polymers diffuse mainly along the direction of their tube in a process called reptation. Stress relaxation after an external perturbation is related to chains escaping from their tubes, a phenomenon known as tube renewal. Currently, the concept of tube models and reptation form the foundation of polymer dynamics and have been used, in modified forms, to understand the behavior of more complex molecules such as star-shaped and branched polymers[4].

When we imagine polymeric materials as spaghetti or similar macroscopic athermal systems, we make an underlying assumption that the topological constraints in the form of entanglements of the molecules is the most important feature. However, despite this assumption being widely accepted, it has not yet been experimentally tested.

In this study, we analyze the topology of macroscopic entangled systems that serve as adequate analogs of polymer melts. Using X-ray tomography, we are able to determine the configuration of individual rubber bands and obtain a comprehensive structural characterization of the assemblies. This provides us with a direct comparison to experimental and simulation results on melts of linear polymers, ultimately furthering our understanding of the entangled structure of polymer melts.

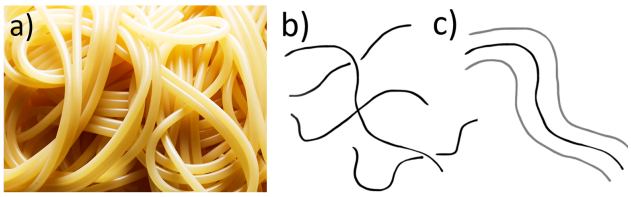

Fig. 1 Polymer analogues. a) - Polymers are often thought to behave like noodles, earthworm swarms, or snakes. b)-c) The structure and dynamics of polymers are described as chains whose motion is confined to a tubular region.

Rubber band assemblies: To create the disordered assemblies of linear rubber bands for our study, we placed each band one by one in a cylindrical container with a radius of 3.25 cm and a height of 7.2 cm. We then applied mechanical agitation by rotating the container at a speed of 50 rpm around an axis passing perpendicularly through the center of mass for 5 minutes[5]. To enhance mixing, the container featured a mobile cap that allowed the bands to rotate in a larger volume. We also attempted to shake the container, like in granular polymers, but our systems dissipated too much energy for this approach to work. After mix-

[a] Institut für Multiscale Simulation, Friedrich-Alexander-Universität Erlangen-Nürnberg, 91052, Erlangen, Germany; E-mail: lgomez@uns.edu.ar
[b] Department of Physics, Universidad Nacional del Sur - IFISUR - CONICET, 8000 Bahía Blanca, Argentina.
[c] Institut Laue-Langevin, 71 Avenue des Martyrs, 38042 Grenoble, France.

View Article Online
DOI: 10.1039/D3SM00148B

Table 1 Rubber band's main geometrical and topological properties

type	N_{bands}	ϕ	L (cm)	s_0(cm^2)	R_g (cm)	R_{ee} (cm)	L_p (cm)	$\langle Z \rangle$	a_{pp} (cm)	b_{pp} (cm)	L_{pp} (cm)
A	130	0.159	20.4	0.014	1.95	4.23	10.99	8.59	1.31	0.07	13.68
B	71	0.172	24.1	0.024	1.78	4.46	10.63	7.68	1.43	0.06	13.90
C	58	0.186	30.4	0.025	2.11	4.43	10.24	9.82	1.16	0.06	16.98
D	28	0.180	63.4	0.024	2.34	4.42	11.65	10.44	1.07	0.04	19.86

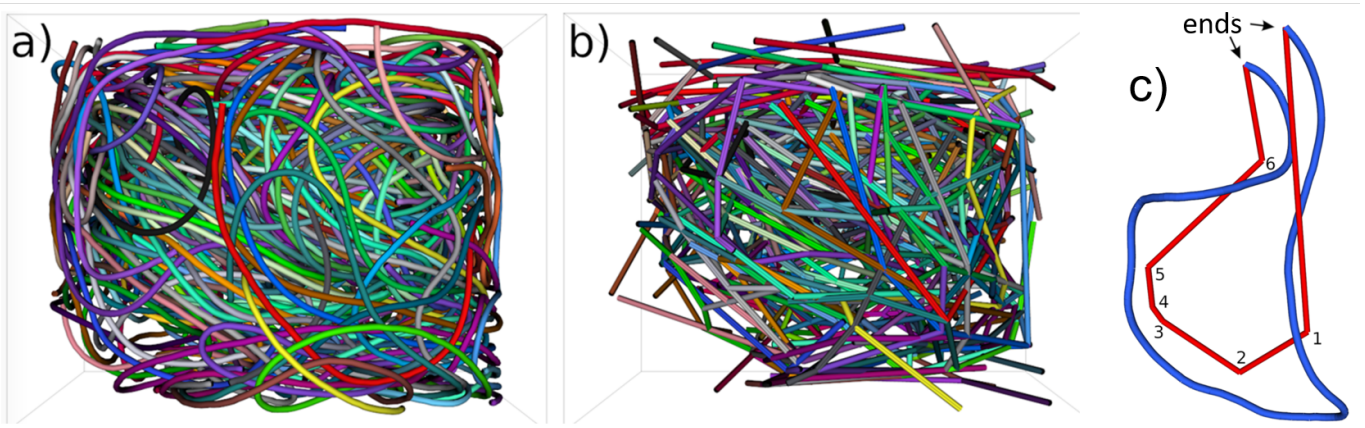

Fig. 2 Topological analysis. a) An assembly of 130 linear bands of type A and b) their Primitive Path (PP) reductions obtained by the $Z1$ algorithm. The label color is preserved between the original bands and the corresponding primitive paths. c) An isolated band of this assembly (in blue) together with its associate PP (in red). The corners in the PP, labelled by numbers, are associated with entanglements. Note that the orientation of the band in panel c) has been inverted due to space limitations (the ends of the band do not rest on the cap of the container, but on the cylindrical wall instead).

ing, we compressed the bands slightly by displacing the cap to reach the final height of 7.2 cm. This simple mixing technique produced disordered packing with reproducible geometrical and topological statistical properties, as described below.

Table 1 presents the key characteristics of the rubber bands used in our study. These include the number of bands (N_{bands}) and packing volume (ϕ) in the assembly, as well as their lengths (L), transverse section (s_0), square root of the mean squared radius of gyration (R_g), square root of the mean squared end-to-end distance (R_{ee}), and persistent length (L_p). Furthermore, Table 1 also includes the main topological features of the assemblies obtained through an entanglement analysis (see below)[6–10]. These features include the average number of entanglements per chain ($\langle Z \rangle$), the effective tube diameter (a_{pp}), and the average contour length (L_{pp}) and bond length (b_{pp}) of the primitive paths. We prepared five assemblies for each of the four band types designated as A to D. All bands used in each type had the same length, ensuring no polydispersity was present.

To analyze the internal structure of the rubber band assemblies, we used X-ray tomography with a CT-Rex device, which had a voxel resolution of 35 μm. The X-ray source was set to a voltage of 100kV and a current of 350 μA. The tomograms were acquired by rotating the samples in 1600 steps (refer to a typical tomogram in the Supplementary Material).

We calculated the packing volume of the structures directly from the tomograms by measuring the volume occupied by the rubber bands relative to the container's total volume. The studied systems had packing volumes ranging from $\phi \sim 0.17$ to 0.18, which allowed them to be mechanically mixed while still being sufficiently dense to approximate polymers.

To analyze the arrangement of the bands within the assembly, we conducted segmentation analysis on the tomograms and transformed the segmented band volumes into an array of beads along their backbones using skeletonization (see supplementary material). This conversion enabled us to represent each band in the assembly as a chain of particles, simplifying the calculation of various geometrical and topological properties. To ensure that neither geometrical nor topological properties were affected, we set the bond length of the chains representing the bands at $l_{beads} \sim 1$mm, which resulted in approximately $N_{beads} \sim 200$, 240, 300, and 630 beads for systems A to E, respectively.

Figure 2a) shows a typical result of our segmentation analysis, applied to an assembly of type A bands, where each band is labeled with a different color for easy visual inspection of their configurations. After identifying all the bands in the system, we moved on to analyzing the entangled structures.

Entanglements: To study the entangled structures, we used a topological analysis similar to those used for studying entanglement in linear polymers in molecular dynamics simulations. The *Z1-algorithm* was applied to find entanglements by performing a series of geometric minimizations, starting by fixing the ends of the chains and disabling excluded volume interactions while preserving the chains' uncrossability condition[6–10]. After applying a series of geometric operations to the chains, the code identified the primitive path (*PP*) for each chain, which is defined as the shortest path connecting the two ends of a chain while maintaining its topology.

The primitive path (PP) is a key concept in the tube model of

Published on 24 April 2023. Downloaded on 4/26/2023 11:22:33 PM.
Soft Matter Accepted Manuscript

View Article Online
DOI: 10.1039/D3SM00148B

Published on 24 April 2023. Downloaded on 4/26/2023 11:22:33 PM.

Edwards[11,12]. The abundance of nearby chains forms a tubular cavity whose central axis is the PP. The Z1-algorithm calculates the statistical properties of this network and the locations of kinks along the three-dimensional PP for each chain[8,9].

Figure 2b shows the PP network for the packing shown in Fig. 2a. In both panels a chain and its PP are drawn in the same color. Note that some PPs remain in the neighborhood of their corresponding chains, since geometric minimization is frustrated by the entanglements. Figure 2c shows one particular chain together with its PP. As per definition, both paths start and end at the same points, namely at the chain ends. We also see that the PP consists of a sequence of straight lines. Numbers along the PP indicate the connections between these segments. At these points called *kinks*, the algorithm cannot proceed with minimization because of the uncrossability condition, since the presence of another PP belonging to another chain inhibits further geometric reduction. In general, the number of kinks is proportional to the number of entanglements Z, and in this context, both terms can be considered interchangeable.

Figure 3 illustrates how the average number of entanglements $\langle Z \rangle$ grows as a function of the length of the bands. To compare entanglements in different systems, we determine the number of strands per volume of the band, given that the bands in System A are considerably thinner. For shorter bands, entanglements increase linearly with the band's length, with entanglements occurring approximately every 3 cm. This linear relationship has been observed in other systems, such as linear Polyethylene chains[13]. However, as shown in Figure 3, for the longest bands, there is a deviation from this linear scaling due to saturation in $\langle Z \rangle$, with entanglements occurring approximately every 6 cm. This saturation is caused by confinement in the packing, which becomes more prominent as the bands get longer.

In addition, the inset of Fig. 3 shows the probability distribution of entanglements in Systems A through D. While the total number of entanglements is not high enough to yield smooth distributions, we observe that for rubber bands like those in System A, which have the greatest number of bands, the distribution appears to approach a Poisson distribution, as predicted for monodisperse linear polymers[13]. It's worth noting that the entanglement analysis is robust with respect to the band's discretization. In general, the number of entanglements in all systems changes only slightly when using a different bond for the chain approximation of bands (see Fig. 3 in the Supplementary Material).

Confinement effects: To delve further into confinement effects, we analyzed the spatial distribution of chain beads, chain ends, and entanglements. Figure 4 displays these distributions as a function of the distance, r, from the center of the cylindrical container. The red lines in the figure's panels represent the values corresponding to a homogeneous distribution of the variables analyzed.

The spatial distribution of chain beads in Fig. 4a reveals a gradual increase in density from the center of the container towards the edge, which is due to the semiflexibility of the ribbons. These ribbons tend to adopt specific configurations to minimize the cost of bending energy, resulting in the observed density increase. Similar observations have been reported in simulations of confined linear and annular polymer molecules[14]. It's important to note that the bead density reaches its maximum near the container and then drops abruptly to lower values. This pattern of maxima and minima near the container is a result of confinement effects from the container and has been observed in Monte Carlo simulations of confined polymer melts[15].

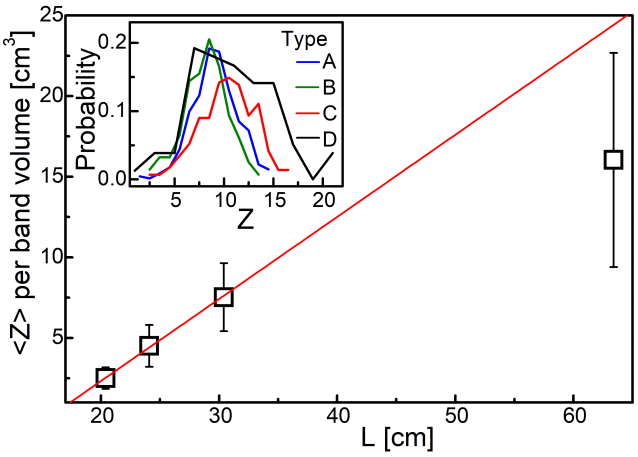

Fig. 3 Entanglements. Average number of entanglements $\langle Z \rangle$ per volume of bands as a function of the band's length L, for the different systems studied. The inset show the probability distribution of entanglements in the different systems.

The spatial distribution of chain ends is depicted in Fig. 4b. Due to the relatively smaller total number of ends, we have averaged over bands of different lengths. We observe that the ends of the bands are preferentially located near the center and edge of the cylinder, which can also be seen from Figures 2a-b. The increased density of chain ends near the surface is a well-known confinement effect that is typically observed in simulations of linear polymers confined in various geometries[16,17].

The accumulation of ends near the surface significantly impacts the properties of polymers, as it modifies the surface tension (which decreases as $1/L$). The initial explanation for this phenomenon was based on the fact that for natural polymers, the monomers at the ends of the chains interact differently with the surface than other monomers. Later, it was shown that entropy could also cause this accumulation. A chain end positioned near the repulsive wall places fewer constraints on the system than a middle monomer placed near the wall.

In semi-flexible polymers, the accumulation of ends towards the edge of the cylinder is also driven by energy since an inner monomer near the surface may require the chain to bend, while an end monomer does not[18]. Our experiments with rubber bands demonstrate that bending energy in macroscopic systems is also significant enough to cause end segregation at the surface.

Finally, Fig. 4c displays the spatial distribution of the entanglements. It can be seen that the density of entanglements approaches zero near the edge of the cylinder. This behavior has also been observed in MD simulations[19]. The decrease in the

Soft Matter Accepted Manuscript

View Article Online
DOI: 10.1039/D3SM00148B

Published on 24 April 2023. Downloaded on 4/26/2023 11:22:33 PM.

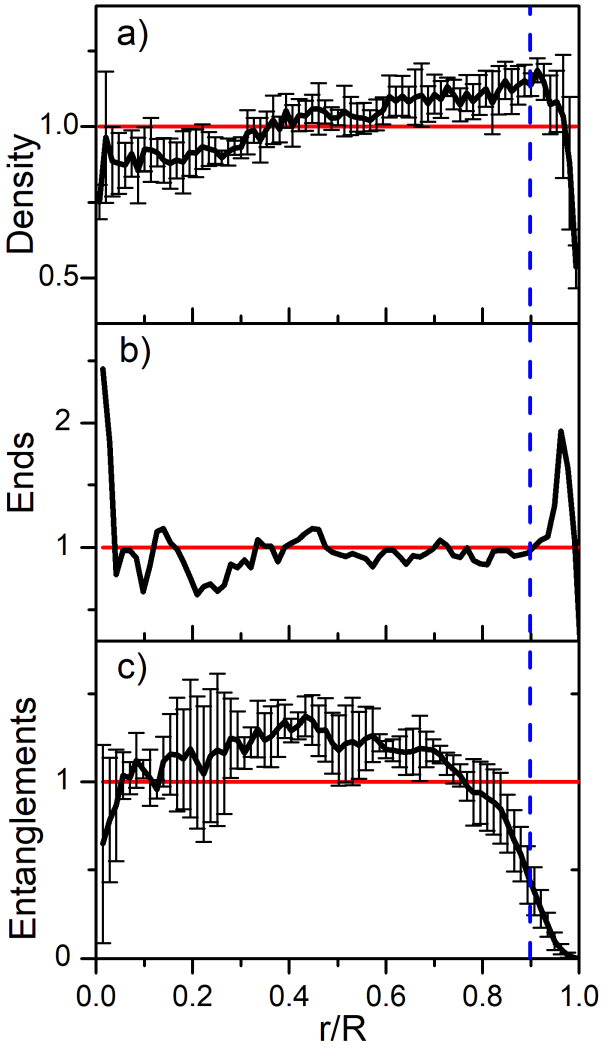

Fig. 4 Confinement effects. Radial distribution of (a) beads, (b) ends, and (c) entanglements. The red lines correspond to homogeneous distributions. The dashed lines demarcate the regions where the influence of the boundary dominates the packing. The black lines show the average over all band lengths, the error bars are obtained from the standard deviations

density of entanglement near the edge is related to the increase in the density of chain ends and decrease in the density of bands. This relationship is illustrated by the blue lines in Fig. 4, which demarcate the region where confinement noticeably impacts the distributions of beads, ends, and entanglements.

Conclusions: Our findings suggest that macroscopic entangled systems, such as noodles, earthworms, snakes, and rubber bands, can effectively serve as models for polymers. This is because the topological constraints on the molecules forms the basis of the entanglement network that controls the mechanical response of polymeric materials. To gain further insights into how entanglement influences the properties of polymers, it would be valuable to investigate the impact of confinement (container size) and packing volume on the scaling regimes of entanglements in macroscopic systems.

It is worth noting that rubber bands have limitations in understanding the dynamic aspects of polymers due to their high level of dissipation. However, other macroscopic chain-like systems may be capable of achieving this. Nonetheless, the study of the configurational properties of rubber bands provides valuable insights into the entanglement behavior of polymers.

Author Contributions

LRG and TP designed research; LRG and NAG performed research; LRG, NAG, and TP analyzed data; and LRG, NAG, and TP wrote the paper.

Conflicts of interest

There are no conflicts to declare.

Acknowledgements

LRG acknowledges support from the Alexander von Humboldt Foundation through the Georg Forster and return fellowships. This work was also supported by the National Research Council of Argentina, CONICET (PIP 112-202001-03059), Universidad Nacional del Sur, German Science Foundation through grant SFB814 founding, and ILL-Grenoble. This work was supported by the BAYLAT (Germany) - CONICET (Argentina) cooperation initiative, the Interdisciplinary Center for Nanostructured Films (IZNF), the Competence Unit for Scientific Computing (CSC), and the Interdisciplinary Center for Functional Particle Systems (FPS) at Friedrich-Alexander-Universität Erlangen- Nürnberg.

Notes and references

1 M. Rubinstein and R. H. Colby, *Polymer Physics*, Oxford University Press, 2003.
2 P.-G. De Gennes, *Physics Today*, 1983, **36**, 33–47.
3 M. Doi and S. F. Edwards, *The Theory of Polymer Dynamics*, Oxford University Press, 1988.
4 T. C. B. McLeish, *Adv. Phys.*, 2002, **51**, 1379–1527.
5 L. R. Gómez, N. A. García and T. Pöschel, *Proc. Natl. Acad. Sci. U.S.A.*, 2020, **117**, 3382–3387.
6 M. Kröger, *Comp. Phys. Comm.*, 2005, **168**, 209–232.
7 M. Kröger, *Computer physics communications*, 2005, **168**, 209–232.
8 S. Shanbhag and M. Kröger, *Macromolecules*, 2007, **40**, 2897–2903.
9 N. C. Karayiannis and M. Kröger, *Int. J. Molec. Sc.*, 2009, **10**, 5054–5089.
10 R. S. Hoy, K. Foteinopoulou and M. Kröger, *Phys. Rev. E*, 2009, **80**, 14–16.
11 S. F. Edwards, *Proceedings of the Physical Society*, 1965, **85**, 613–624.
12 S. F. Edwards, *Proc. Phys. Soc. London*, 1967, **92**, 9–16.
13 K. Foteinopoulou, N. C. Karayiannis, M. Laso and M. Kröger, *The Journal of Physical Chemistry B*, 2009, **113**, 442–455.
14 J. Z. Chen, *Prog. Polym. Sci.*, 2016, **54**, 3–46.
15 K. Foteinopoulou, N. C. Karayiannis and M. Laso, *Chemical Engineering Science*, 2015, **121**, 118–132.
16 D. T. Wu, G. H. Fredrickson, J.-P. Carton, A. Ajdari and

Soft Matter Accepted Manuscript

View Article Online
DOI: 10.1039/D3SM00148B

L. Leibler, *J. Polym. Sci., Part B: Polym. Phys.*, 1995, **33**, 2373–2389.

17 M. Matsen and P. Mahmoudi, *The European Physical Journal E*, 2014, **37**, 1–8.

18 S. Blaber, P. Mahmoudi, R. K. W. Spencer and M. W. Matsen, *J. Chem. Phys.*, 2019, **150**, 014904.

19 N. A. García and J.-L. Barrat, *Macromolecules*, 2018, **51**, 9850–9860.

Published on 24 April 2023. Downloaded on 4/26/2023 11:22:33 PM.

Soft Matter Accepted Manuscript